6-2023

Catalyzed Oxidation of IG-110 Nuclear Graphite by Simulated Fission Products Ag and Pd Nanoparticles

Junhua Jiang
Idaho National Laboratory

John Stempien
Idaho National Laboratory

Yaqiao Wu
Boise State University

Publication Information

Jiang, Junhua; Stempien, John; and Wu, Yaqiao. (2023). "Catalyzed Oxidation of IG-110 Nuclear Graphite by Simulated Fission Products Ag and Pd Nanoparticles". *Nuclear Materials and Energy, 35*, 101438. https://doi.org/10.1016/j.nme.2023.101438

Nuclear Materials and Energy 35 (2023) 101438

Contents lists available at ScienceDirect

Nuclear Materials and Energy

journal homepage: www.elsevier.com/locate/nme

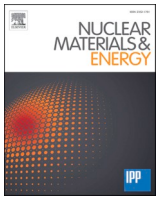

Catalyzed oxidation of IG-110 nuclear graphite by simulated fission products Ag and Pd nanoparticles

Junhua Jiang [a,*], John Stempien [a], Yaqiao Wu [b]

[a] Nuclear Science & Technology Directorate, Idaho National Laboratory, Idaho Falls, ID 83415, USA
[b] Micron School of Materials Science and Engineering, Boise State University, Boise, ID 83725, and Center for Advanced Energy Studies, Idaho Falls, ID 83401, USA

ARTICLE INFO

Keywords:
High temperature gas reactor
Air ingress
Nuclear graphite
Fission products
Catalytic oxidation

ABSTRACT

To evaluate the stability of nuclear materials in high temperature gas reactors under air ingress conditions, catalytic oxidation of IG-110 graphite by two simulated fission products, metallic Pd and Ag, was studied in oxidative atmosphere and at temperatures up to 1000 °C using an integrated furnace, mass spectroscopy and infrared spectroscopy system. Transmission electron microscopy and X-ray diffraction studies show that Pd and Ag nanoparticles were successfully introduced onto powdery IG-110 graphite through an impregnation and subsequent heat-treatment process. The combined mass spectroscopy and infrared spectroscopy methods allow simultaneous analysis of two gaseous products, CO and CO_2, and separate measurements of activation energy for their formation reactions. It was found that the introduction of Pd or Ag to IG-110 graphite substantially catalyzed the oxidation of graphite, characteristic of decreased onset temperatures for the oxidation of graphite. Moreover, the catalytic effects by Pd and Ag are considerably different based on measured concentration ratios of CO_2 to CO as a function of oxidation temperatures. Ag makes the graphite oxidation commence at approximately 400 °C with CO_2 being the dominant product. In contrast, Pd significantly increases the concentration ratio of CO_2 to CO at temperatures higher than approximately 690 °C, although it decreases the onset temperature for the oxidation reaction to around 525 °C. To understand the catalytic difference, the mechanism of the graphite oxidation is discussed based on the changes of surface oxygen species on Ag and Pd.

1. Introduction

High temperature gas-cooled reactors (HTGRs), which are developed to operate in the coolant outlet temperature range between 600 and 1000 °C, represents one of the front-runner Generation-IV reactors because of their inherent safety and high thermal efficiency attributes. To boost the deployment of HTGRs, considerable efforts have been made to evaluate the durability of core structural and fuel materials under operation and design-basis-accident conditions [1,2]. Nuclear graphite has been widely used in HTGRs as a structural material, moderator, and fuel element. In an air ingress accident, graphite will react with molecular O_2 at high temperatures, seriously damaging its mechanical and thermal properties and introducing safety concerns. Therefore, the oxidation of nuclear graphite has been theoretically and experimentally studied under different oxidative conditions [3–5]. Generally, the oxidation behavior is strongly dependent upon reaction temperatures. Considerable oxidation of commonly studied nuclear graphite such as IG-110 and IG-430 occurs at approximately 700 °C [6–8]. At higher temperatures, the oxidation rates are significantly increased [7,8]. Based on the temperature dependence of the reaction rates, activation energy values were calculated and determined to fall within a wide range extending from around 160 to 400 kJ/mol, depending on experimental conditions and methods [8,9]. To understand the oxidation behavior, several different models have been proposed [10,11]. The oxidation of graphite is divided into three regimes: a chemical kinetics-controlled regime at low temperatures, an in-pore diffusion-controlled regime at intermediate temperatures, and a boundary layer-controlled regime at high temperatures. Because molecular O_2 participates in the oxidation of graphite to CO and CO_2, an oxygen transfer model was developed to elucidate the reaction mechanism [12]. The oxidation kinetics are determined by the microstructures of graphite surfaces, surface absorption/desorption of oxygen-containing species, and their surface diffusion. In addition, computational simulation and modeling was conducted to understand the oxidation reactions at multiple length scales [13,14]. However, most of the studies described above are based on the use of high-purity nuclear graphite.

* Corresponding author at: Advanced and Energy Materials Department, Savannah River National Laboratory, Aiken, SC 29808, USA.
E-mail address: junhua.jiang@srnl.doe.gov (J. Jiang).

https://doi.org/10.1016/j.nme.2023.101438
Received 16 September 2022; Received in revised form 10 April 2023; Accepted 28 April 2023
Available online 16 May 2023

During HTGR operations, a range of fission products are generated and a limited amount of some fission products can diffuse from fuels to graphite-based matrix [15,16]. Therefore, the release and transport of fission products from tri-structural isotropic (TRISO) particle fuel have been intensively studied to boost the development and implementation of HTGRs [17–20]. The TRISO kernel is encapsulated by three layers of carbon- and ceramic-based materials that limit the release of radioactive fission products under all reactor conditions. At temperatures higher than approximately 1100 °C, fission products Ag, Sr, Eu, and Pd are likely to be released in their metallic forms. Moreover, their release rates are significantly higher with increasing temperatures [21]. Their transport and sorption in carbon materials and silicon carbide have been carefully examined [22,23]. The diffusion of Ag through intact TRISO fuel particles is a well-documented phenomenon [24]. Recent studies suggest that the significant attack of Pd on SiC may facilitate the diffusion of Ag through the intact SiC layer [24,25]. Therefore, Ag and Pd could eventually diffuse into surrounding fuel matrix and structural graphite in HTGRs. To understand the diffusion of Ag and the migration of Pd, their effective diffusion coefficients in IG-110 graphite were measured [26]. In particular, the sorption of fission products in carbon materials was reviewed [27]. It is suggested that the parameters of carbon structures and irradiation level likely play a dominant role in the sorption. High-temperature isotherms of Ag on nuclear graphite NBG-17 were measured to estimate its adsorption heat [28].

Earlier studies of the oxidation of various carbon materials revealed that the oxidation reaction can be substantially promoted by the introduction of efficient catalysts which include transition metal oxides, inorganic salts, and noble metals [29,30]. Among reported catalysts, Pd and Ag exhibit pronounced catalytic effects to not only the oxidation of carbonaceous materials (such as soot particles and carbon nanotubes) but also the oxidative conversion of CO to CO_2 [31,32]. In contrast, their catalytic effects to the oxidation of graphite—especially that of nuclear graphite—have been rarely studied. Therefore, there is interest to investigate the oxidation of HTGR materials containing fission products under air ingress conditions.

The purpose of the present work was to evaluate the oxidation of IG-110 nuclear graphite modified with metallic Pd and Ag nanoparticles, in an oxidative atmosphere at temperatures correlating to the operation of HTGRs. It was found that Pd and Ag catalyze the oxidation of graphite to CO_2 and CO differently. Ag significantly decreases the onset temperature of the graphite oxidation to approximately 400 °C with CO_2 being the dominant product. In contrast, Pd exhibits significant catalytic effect to the oxidation of graphite to CO_2 at temperatures higher than approximately 700 °C. Furthermore, the values of activation energy for the oxidation of graphite to CO and CO_2 were separately calculated, and the temperature dependence of molar ratio of the products CO_2 to CO was also determined. Therefore, this study will provide an effective method to evaluate TRISO materials under simulated air ingress conditions and the results explain the oxidation behavior of nuclear graphite at temperatures correlated to the operation of HTGRs.

2. Experimental

2.1. Introduction of Pd and Ag nanoparticles to IG-110 graphite

As-received nuclear-grade graphite IG-110 (Toyo Tanso) which is fine-grained isotropic graphite, was ball-milled into powder and sized using mesh sieves. The modification of graphite powder with Pd and Ag nanoparticles followed an impregnation and heat-treatment procedure. To obtain the designed loading of 1 wt% Ag on graphite, 1 wt% $AgNO_3$ solution was added to the graphite powder. The mixture was first dried at room temperature, followed by further drying in an oven at 80 °C. The dried mixture was then transferred into a tube furnace and heat-treated under an Ar flow with a temperature range increasing from room temperature to 600 °C at 3.7 °C/min, holding at 600 °C for 3 h, and subsequent cooling down to room temperature at 3.7 °C/min. There is no safety concern during the drying and heat-treatment. The resulting powdery solids were then pressed into disc samples using a 0.25 cm diameter stainless steel die and a force of 3000 kg for the studies of oxidation reactions. The preparation of graphite powder loaded with 1 wt% Pd followed the same procedure described as above, except the use of a solution of 1 wt% $PdCl_2$ + 5 wt% HCl during the impregnation.

For simplification thereafter, powdery graphite, Pd-modified graphite, and Ag-modified graphite were denoted as IG-110, Pd-IG110, and Ag-IG110, respectively.

2.2. Oxidation studies

The graphite oxidation was studied using an integrated system comprised of a horizontal tube furnace (Model 1630-12HT, CM Furnaces Inc.) and an HPR-20 R&D analyzer equipped with HAL/3F 201 RC triple filter mass spectrometer (MS) using Faraday/Multiplier detector (Hiden Analytical Limited) and a mass range of 0 to 100 amu, as shown in Fig. 1. To reliably analyze the gaseous product CO without the inference of N_2, a CO analyzer (Thermo Scientific Model 48i-TLE) was coupled to the MS unit. Two gas streams, high-purity Ar and a customized gas of 6.7 vol% O_2 balanced by helium (He), were separately controlled using Bronkhorst mass flow controllers and an E-8000 series digital readout/control system. The tube furnace was controlled using a control system consisting of a 2404 EUROTHERM temperature controller, SCM power controller, and over-temperature protector. Hiden QGA quantitative gas analysis software was used for quantitative analysis of multicomponent gases.

During each oxidation run, a high-purity alumina boat holding a pressed sample was placed in the center zone of the furnace tube and a gas flow of 1500 SCCM consisting of 300 SCCM O_2-He and 1200 SCCM Ar was introduced to flow through the tube. The temperature was increased from room temperature to 1000 °C at a ramp rate of 3.7 °C/min. The gases exiting the tube were analyzed continuously by the MS and CO analyzer as the temperature was rising.

The changes of Gibbs energy for the oxidation of graphite and the transformation of Ag and Pd components induced by molecular O_2, CO, or CO_2 were analyzed using HSC Chemistry® 10 software [33] and a thermochemical diagrams module containing a database of enthalpy, entropy, heat capacity, Gibbs energy, and exergy for different chemical species.

2.3. Characterization of Ag and Pd impregnated graphite

The characterization of IG-110, Pd-IG110, and Ag-IG110 was performed prior to oxidation tests using a scanning-electron-microscope (SEM), energy-dispersive X-ray spectroscopy (EDS), X-ray powder diffraction (XRD), and transmission electron microscopy (TEM) at the Microscopy and Characterization Suite (MaCS) of the Center for Advanced Energy Studies (CAES). The crystalline structures of the samples were examined in the 2θ range from 15° to 85° at a scanning speed of 2°/min using a Rigaku Smartlab X-ray diffractometer with Ni filtered Cu Kα radiation operated at 40 kV and 40 mA, and PDXL software. SEM and EDS measurements were performed using a JEOL JSM 6610LV SEM equipped with an EDS detector. TEM samples were prepared by diluting the ink with isopropyl alcohol and drop casting onto a 300 mesh TEM Cu grid coated with a carbon support film. TEM imaging studies were carried out using a FEI Tecnai G2 F30 STwin scanning transmission electron microscope operated at 300 kV. FEI TIA (ESVison) software was employed to analyze EDS data.

3. Results and discussion

3.1. Characterization of IG-110, Pd-IG110, and Ag-IG110

Fig. 2 shows SEM images of pressed samples prior to oxidation for IG-110, Pd-IG110, and Ag-IG110. They show similar irregular appearance

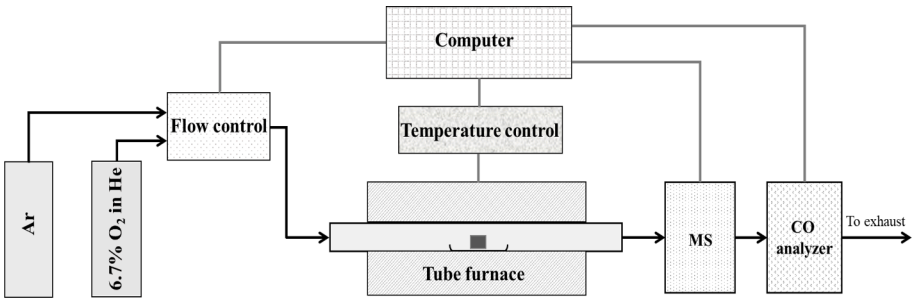

Fig. 1. Schematic setup for the studies of graphite oxidation using an integrated tube furnace, mass spectrometer, and CO analyzer.

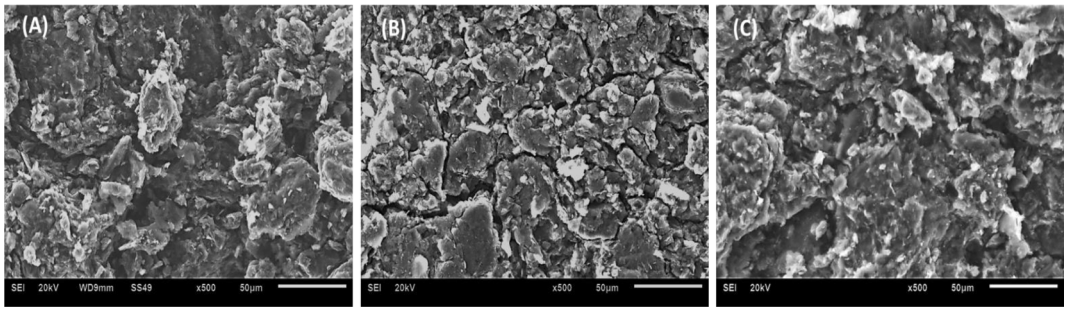

Fig. 2. SEM images of pressed IG-110 (A), Pd-IG110 (B), and Ag-IG110 (C).

and a wide particle size distribution. The EDS spectra for the three samples measured in selected areas that have fine and large particles are shown in Fig. 3. IG-110 contains 100 wt% C. Pd-IG110 and Ag-IG110 exhibit L_α and L_β peaks corresponding to Pd and Ag, respectively. Their loadings are approximately 1.2 wt% Pd for Pd-IG110 and 0.9 wt% Ag for Ag-IG110, estimated from the EDS spectra performed on areas of around 50 μm × 50 μm. A more accurate analysis of Pd and Ag elements in the samples could be obtained using glow discharge mass spectrometry or through appropriate sample digestion followed by inductively coupled plasma optical emission spectrometry or mass spectrometry.

Spot EDS analysis performed on selected bright fine particles in Fig. 2 (B) and (C) indicates that some of them are likely to be Pd or Ag particles. To examine the crystalline structures of Pd and Ag supported on IG-110, the XRD patterns of IG-110, Pd-IG110 and Ag-IG110 were measured in the 2θ range from 15° to 85° and they are shown in Fig. 4. IG-110 exhibits diffraction peaks at 2θ = 26.6°, 42.7°, 44.7°, 54.8°, 59.9°, 77.7°, and 83.9°. These values are consistent with literature data

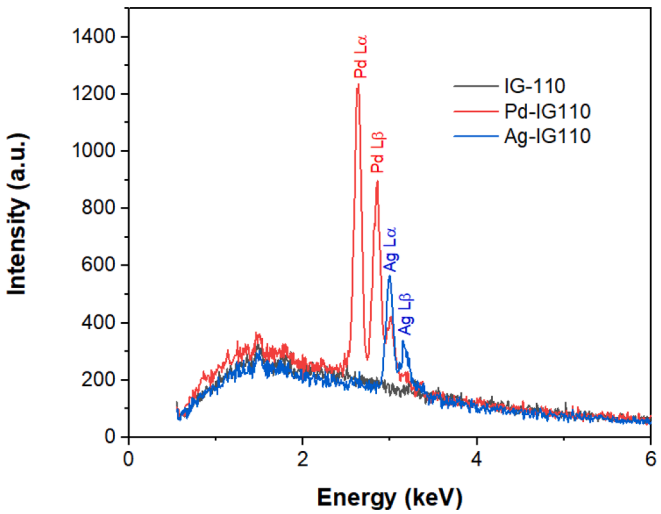

Fig. 3. EDS spectra of IG-110, Pd-IG110, and Ag-IG110.

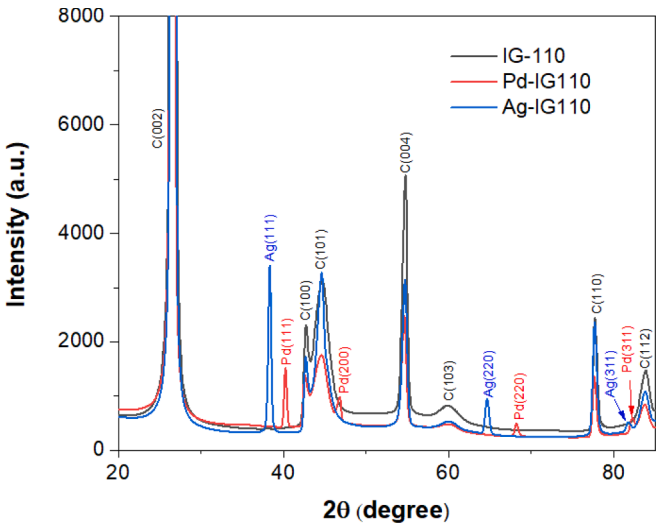

Fig. 4. XRD spectra of IG-110, Pd-IG110, and Ag-IG110.

for IG-110 graphite [34]. They can be assigned to C(002), C(100), C(101), C(004), C(103), C(110), and C(112) planes, respectively. For Pd-IG110, four new peaks at 2θ = 40.2°, 46.8°, 68.2°, and 82.2° were observed. They correspond to (111), (200), (220), and (311) planes of polycrystalline Pd with face centered cubic (*fcc*) crystalline structure [35]. Similarly, Ag-IG110 generates three new peaks at 2θ = 38.4°, 64.7° and 81.8°, corresponding to Ag(111), Ag(220) and Ag(311) facets, respectively [36]. Therefore, the XRD studies of three samples suggest that metallic Pd and Ag particles are formed on IG-110 through the impregnation and heat-treatment procedure.

The crystalline sizes (d) of Pd and Ag particles can be estimated according to Debye-Scherrer's formula as follows [37]:

$$d = \frac{0.89\lambda}{\beta_{2\theta} cos\theta} \quad (1)$$

where λ is the X-ray wavelength (0.15418 nm), θ is the Bragg diffraction angle, and $\beta_{2\theta}$ is the full peak width at half-maximum. The calculated crystallize sizes for Pd and Ag particles based on their peak broadening profile of (1 1 1) peak are approximately 22.1 and 21.4 nm, respectively.

The particle sizes of Pd and Ag on IG-110 and their dispersions were examined using TEM. The dark-field and bright-field TEM images and electron diffraction patterns for Pd-IG110 and Ag-IG110 are shown in Fig. 5(A) and (B) respectively. Fig. 5(A) exhibits aggregated and highly dispersed Pd. The equivalent size of the largest particle in the aggregate is about 300 nm. In the highly dispersed region, the particle sizes fall in a range of approximately 2 to 20 nm. The electron diffraction patterns at a selected area can be indexed to (111), (200), (220), and (311), consistent with the XRD results shown in Fig. 4. Compared to Pd-IG110, higher dispersion was observed on Ag-IG110. Fig. 5(B) shows smaller aggregates. The equivalent sizes of well dispersed particles are in the range of around 30 and 120 nm. The electron diffraction patterns are consistent with those of Ag crystalline indices, albeit with some interference of crystalline IG-110.

3.2. Oxidation of IG-110, Pd-IG110, and Ag-IG110

Fig. 6 shows the temperature dependence of CO and CO_2 concentrations for IG-110, Pd-IG110, and Ag-IG110. For comparison, each measured concentration in ppm was normalized to the geometric surface area exposed to the oxidative flow for a disc sample (which includes the top circular area and the cylinder-side area, and the density is approximately 1.44 g/cm^3). The oxidation of IG-110 to both CO and CO_2 commences at approximately 650 °C. Their concentrations significantly increase with increasing temperatures until their values are maximized. For the CO formation, the peak concentration is approximately 155 ppm/cm^2 at 776 °C. When the temperature is further increased to 1000 °C, the CO concentration gradually decreases. The CO_2 concentration is maximized to around 909 ppm/cm^2 when the temperature is increased to 906 °C. A plateau with slight concentration decline is seen at higher temperatures. In the oxidation, the concentration of molecular O_2 was also measured as a function of reaction temperature. The initial concentration is approximately 6100 ppm/cm^2. It starts to decrease at approximately 650 °C where the oxidation of graphite occurs and reaches a minimum of approximately 5200 ppm/cm^2 when the CO_2 concentration is maximized at 909 ppm/cm^2. Therefore, the consumption of O_2 is not significant during the oxidation.

The introduction of Pd and Ag substantially changes the characteristics of the concentration-temperature dependence. For Pd-IG110, the onset temperatures for the CO and CO_2 formation are approximately 525 and 590 °C, respectively. The CO concentration increases along with the temperature until it is maximized at 668 °C. A considerable decrease in the concentration is observed when the temperature is increased to about 700 °C, followed by gradual decrease at higher temperatures up to 1000 °C. The CO_2 concentration is substantially increased with rising temperatures until a concentration plateau appears at temperatures higher than approximately 835 °C.

For Ag-IG110, the distinguishing characteristic from those for IG-110 and Pd-IG110 is that the onset temperature for the CO_2 formation is only 400 °C and the CO concentration is negligible at this temperature. Increasing temperature significantly increases the CO_2 concentration and produces two concentration waves. One is seen between approximately 580 and 763 °C with a value of around 600 ppm/cm^2 and another is seen between approximately 849 and 946 °C with a value of about 811 ppm/cm^2. The CO formation exhibits a symmetric peak-shaped temperature dependence, characteristic of an onset temperature at 608 °C and a peak temperature at 774 °C, with a high peak concentration of about 262 ppm/cm^2.

Based on the above results, the characteristic parameters for the oxidation of CO and CO_2 on IG-110, Pd-IG110 and Ag-IG110, including their corresponding onset temperatures, peak temperatures, and peak concentrations are included in Table 1.

The temperature dependence of the sum of CO and CO_2 concentrations indicates that the oxidation of graphite to CO_2 becomes gradually dominant on IG-110, Pd-IG110, and Ag-IG110 when the temperatures are higher than the peak temperatures for the CO formation.

The correlation of the rates of the graphite oxidation reactions for the CO and CO_2 formation in this case can be described as follows:

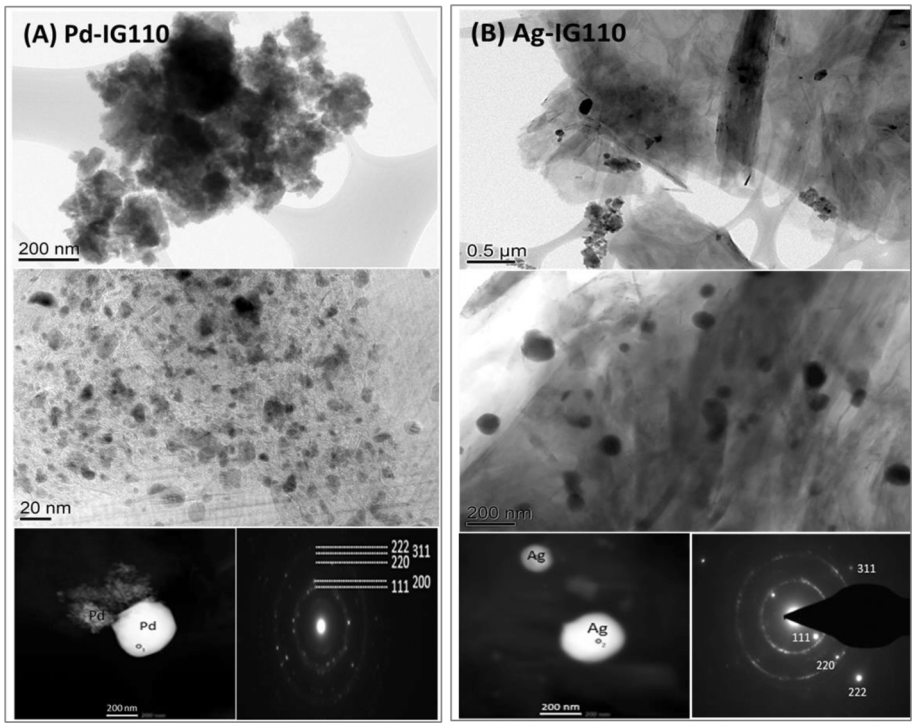

Fig. 5. Dark-field and bright-field TEM images and selected area electron diffraction of Pd-IG110 (A) and Ag-IG110 (B).

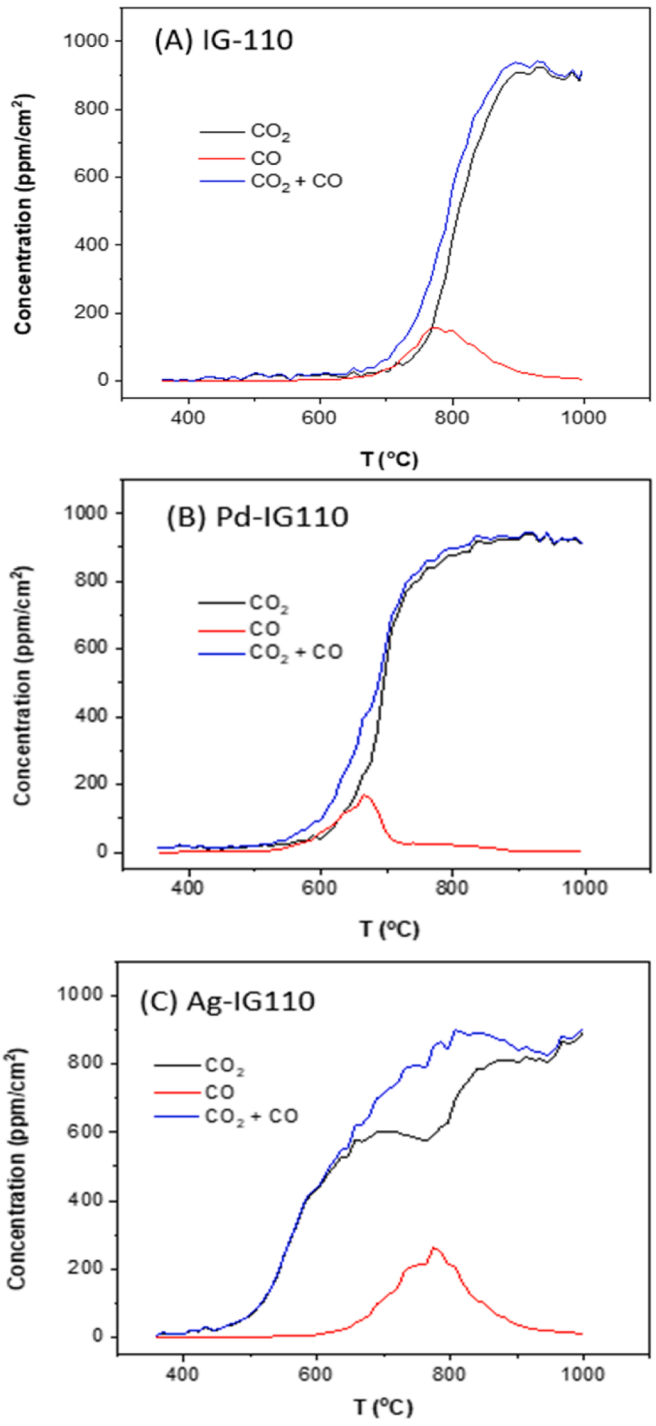

Fig. 6. Temperature dependence of CO_2 and CO concentration during graphite oxidation. (A) IG-110; (B) Pd-IG110; and (C) Ag-IG110.

$$k_{CO} = \frac{100 \times [CO] \times \rho \times Q}{A \times M_{CO}} \tag{2}$$

$$k_{CO_2} = \frac{100 \times [CO_2] \times \rho \times Q}{A \times M_{CO_2}} \tag{3}$$

where k_{CO} and k_{CO_2} are the reaction rate for the CO and CO_2 formation (in mol/cm^2 s), [CO] and [CO_2] are the CO and CO_2 concentrations (in *ppm*), ρ is the density of the oxidative gas mixture (in g/cm^3), Q is the flow rate of the gas mixture (in cm^3/s), A is the geometric surface area of the sample (in cm^2), M_{CO} and M_{CO_2} are the molar mass of CO and CO_2 (in g/mol) respectively.

3.3. Reaction activation energy

The values of activation energy for the oxidation of graphite to CO and CO_2 based on Equations (4) and (5):

$$k_{CO} = k_{o,CO} \times e^{\left(-\frac{E_{a,CO}}{RT}\right)} \tag{4}$$

$$k_{CO_2} = k_{o,CO_2} \times e^{\left(-\frac{E_{a,CO_2}}{RT}\right)} \tag{5}$$

where $E_{a,CO}$ and E_{a,CO_2} are the activation energy (in kJ/mol), $k_{o,CO}$ and k_{o,CO_2} are the pre-exponential factors, and other terms have their normal meanings. By combing Equations (2) ~ 5, the concentration dependence of activation energy can be written as

$$\ln([CO]) = B_{CO} - \frac{E_{a,CO}}{RT} \tag{6}$$

$$\ln([CO_2]) = B_{CO_2} - \frac{E_{a,CO_2}}{RT} \tag{7}$$

where B_{CO} and B_{CO2} are the constants independent of [CO] and [CO_2], which incorporate their corresponding pre-exponential factors.

The Arrhenius plots for the formation of CO and CO_2 on IG-110, Pd-IG110, and Ag-IG110 are shown in Fig. 7. The temperature dependence of logarithm of [CO_2] exhibits similar linear regions in the lower temperature ranges for the three samples, followed by the less-temperature dependent regions at the higher temperature ranges which is related to mass transport limitation of O_2. This dependence is similar to the literature results for IG-110 graphite [38]. In contrast, the temperature dependence of the logarithm of [CO] shows local maxima near the middle of the temperature range. They are comprised of linear rising regions in the lower temperature ranges, maximized concentrations, and decreasing regions in the higher temperature ranges. Compared to IG-110, the influences of adding Pd and Ag to IG-110 are different. The higher temperature region of 500 to 1000 °C on Pd-IG110 is comprised of approximately four sub-regions. The low-temperature region of approximately 450 to 550 °C in which the CO concentration linearly rising for Ag-IG110 is considerably separated from that for the CO_2 formation with a temperature difference of approximately 170 °C.

The activation energy for the CO and CO_2 formation on each sample can be separately estimated from their corresponding low-temperature linear regions. Their values ($E_{a,CO}$ and E_{a,CO_2}) are provided in Table 2. For IG-110, the E_{a,CO_2} and $E_{a,CO}$ values are approximately 250.2 and 196.9 kJ/mol, respectively. In the literature, the activation energy for the oxidation of IG-110 under varying conditions has been normally measured according to the mass changes of a graphite sample during oxidation as a function of temperatures [6–9]. The reported values are

Table 1
Onset temperatures (T_o), peak temperatures (T_p), peak or plateau concentrations for the formation of CO and CO_2.

	$T_{o,\ CO}$ (°C)	$T_{p,\ CO}$ (°C)	$[CO]_{peak}$ (ppm/cm^2)	$T_{o,\ CO2}$ (°C)	$[CO_2]_{plateau}$ (ppm/cm^2)
IG-110	650	776	155	705	903
Pd-IG110	525	668	168	590	908
Ag-IG110	608	774	262	400	601, 811

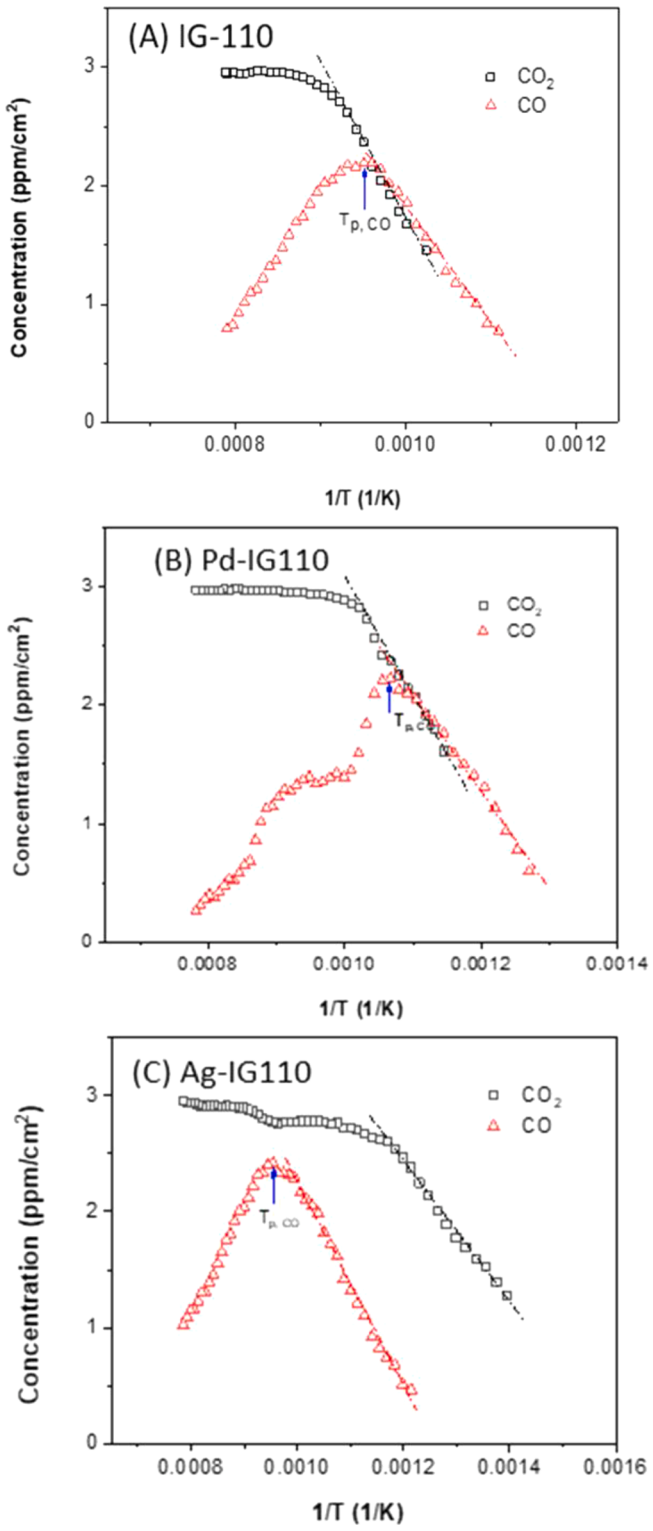

Fig. 7. Arrhenius plots of CO_2 and CO concentration as a function of inverse temperature. (A) IG-110; (B) Pd-IG110; and (C) Ag-IG110.

within a wide range of 160 to 400 kJ/mol. One of the reasons for the wide variance may be the use of different temperature ranges. However, the individual measurements of $E_{a,CO}$ and E_{a,CO_2} have rarely been reported. In contrast, the values of $E_{a,CO}$ and E_{a,CO_2} were determined in this study according to the individual changes of [CO] and [CO_2] with increasing temperature. The simultaneous determination of $E_{a,CO}$ and E_{a,CO_2} makes it possible to analyze the oxidation of graphite to CO and CO_2 under the same conditions, the relative amounts of CO and CO_2 produced, and the competition between their formation reactions.

Table 2
Calculated values of activation energy (E_a) for the oxidation of IG-110, Pd-IG110, and Ag-IG110 to CO_2 and CO.

	E_a for oxidation to CO_2 (kJ/mol)	E_a for oxidation to CO (kJ/mol)
IG-110	250.2 ± 0.1	196.9 ± 0.2
Pd-IG110	171.9 ± 0.1	166.0 ± 0.1
Ag-IG110	107.6 ± 0.1	169.6 ± 0.1

The introduction of Pd and Ag effectively decreases the values of the $E_{a,CO}$ and E_{a,CO_2}. The $E_{a,CO}$ values are 166.0 for Pd-IG110 and 169.6 kJ/mol for Ag-IG110. Their E_{a,CO_2} values are 171.9 and 107.6 kJ/mol, respectively. These values indicate that Pd and Ag can efficiently catalyze the oxidation of IG-110 to both CO and CO_2. Moreover, Ag is highly active, and therefore catalyzes the oxidation of graphite to CO_2 commencing at approximately 400 °C.

3.4. Temperature dependence of concentration ratio of CO_2 to CO

The intrinsic oxidation of graphite in O_2 is described as follows:

$C + 0.5(1 + \chi)O_2 = \chi CO_2 + (1\text{-}\chi)CO$(I)

where χ is the molar fraction of CO_2 in the mixture of CO and CO_2. The ratio of χ to (1-χ) is equal to the molar ratio of CO_2 to CO. Its temperature dependence can be determined from the variations of [CO_2] and [CO] with temperatures according to Equation (8), as shown in Fig. 8(B).

$$\frac{\chi}{1-\chi} = \frac{[CO_2]M_{CO}}{[CO]M_{CO_2}} \tag{8}$$

Generally, the dependence for IG-110 shows the gradual increase of CO_2 fraction with increasing temperature when the temperature is higher than 736 °C, following a slight decrease in the lower temperature range. At 1000 °C, the ratio is maximized to approximately 114. On Pd-IG110, the CO_2-to-CO ratio shows an approximate three-stage temperature dependence at temperatures higher than 685 °C: an initial rise between 685 and 728 °C, a gradual increase between 728 and 835 °C, and a rapid increase from approximately 35 to 324 when the temperature is further increased to 1000 °C. A different dependence is observed on Ag-IG110, exhibiting the peak-shaped response over a wide range between 400 and 775 °C and gradual increase when the temperature is further increased. The peak ratio is approximately 56.4 at 561 °C, the lowest value is about 1.4 at 775 °C, and a value at 1000 °C is 53.3. The molar fraction of CO_2 as a function of temperature is shown in Fig. 8(A). However, it is clearly observed that the lowest χ values for the three samples are: 0.30 at 725 °C for IG-110, 0.30 at 600 °C for Pd-IG110, and 0.59 at 775 °C for Ag-IG110. All χ values at 1000 °C approach 1.0 indicative of nearly 100% CO_2 as the oxidation product. For Ag-IG110, the χ values higher than 0.97 at temperatures lower than around 600 °C also indicate that the main reaction is the oxidation of graphite to CO_2.

Based on Equations (2)–(5) and 8, the temperature dependence of χ/(1-χ) can be written as:

$$\ln\left(\frac{\chi}{1-\chi}\right) = \ln\left(\frac{k_{o,CO_2}}{k_{o,CO}}\right) + \frac{(E_{a,CO} - E_{a,CO_2})}{RT} \tag{9}$$

This equation indicates that the temperature dependence of the χ/(1-χ) ratio is likely to follow an Arrhenius behavior. In the plot of logarithmic ratio versus reciprocal temperature in Kelvin (Fig. 9), IG-110 and Ag-IG110 exhibit linear relationships at temperatures higher than 785 °C. However, no linear relation can be drawn for Pd-IG110 in the similar temperature range. Instead, a three-region dependence was observed. This may indicate the complexity of the oxidation reaction. In the above temperature range, the oxidation of CO to CO_2 (Reaction II) is spontaneous. In addition, the reaction of CO_2 and C becomes likely (Reaction III) when the temperature is higher than approximately

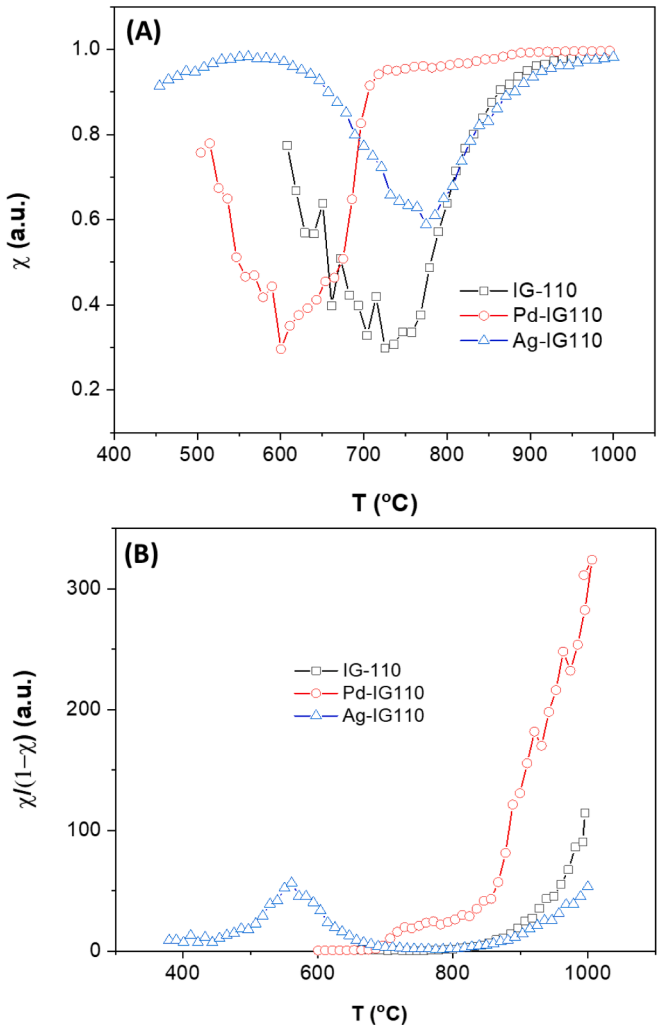

Fig. 8. (A) Temperature dependence of CO_2 fraction in the mixture of CO and CO_2 during the oxidation of IG-110, Pd-IG110 and Ag-IG110; (B) temperature dependence of concentration ratio of CO_2 to CO.

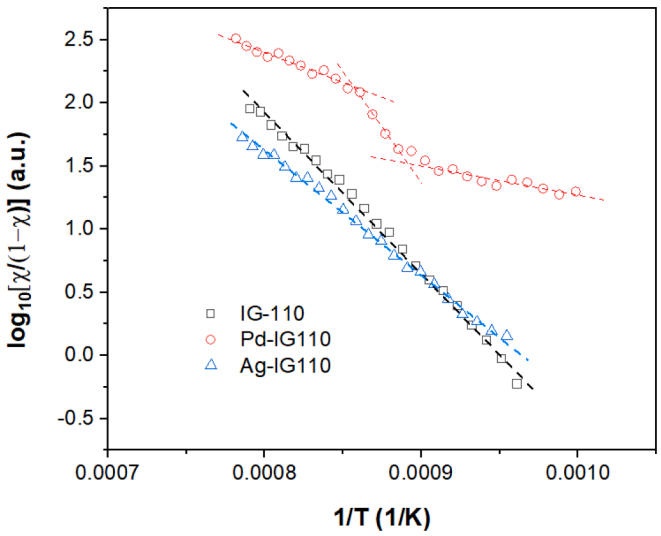

Fig. 9. Arrhenius plots for the molar ratio of CO_2 to CO in the mixture on IG-110, Pd-IG110, and Ag-IG110.

700 °C. If Reaction II or III occurs, there is a need to modify Equations 2 or 3, which is likely to result in some deviation from a linear relation predicted by Equation (9). Moreover, Reaction III can also be catalyzed by Pd or Ag, as discussed in the following sections.

$C + CO_2 = 2CO$(II).

$CO + 0.5O_2 = CO_2$(III).

In the literature, the values of the CO_2 to CO ratio were measured during the oxidation of graphite within the range between 520 and 1420 °C and several empirical correlations between the ratio and temperatures were suggested [6,39,40]. In this case, Equation (9) provides the physical meaning for the temperature dependence of the ratio. On IG-110 and Ag-IG110, the linear regions could be attributed to the difference of activation energy for the CO_2 and CO formation.

3.5. Catalytic effects by Pd and Ag

Fig. 10 shows the variations of Gibbs energy for the oxidation of graphite to CO and CO_2 (via Reactions IV and V) and the oxidation of CO to CO_2 (Reaction III) in the temperature range of 20 and 1000 °C. All their values are negative, indicative of thermodynamical spontaneousness for Reactions III ~ V. The Gibbs energy for the reaction between graphite and CO_2 (Reaction II) is strongly temperature dependent. The zero value is seen at approximately 700 °C. At higher temperatures, it turns positive, indicating that Reaction II becomes thermodynamically unfavored.

$C + O_2 = CO$(IV).

$C + 0.5O_2 = CO$(V).

The reaction mechanism of nuclear graphite oxidation in molecular O_2 has been discussed frequently based on several reaction kinetics models [41–46]. It is accepted that graphite can be oxidized to CO and CO_2 through multiple pathways, depending on several factors which may include the activity and microstructures of graphite surfaces, driving forces such as temperature and pressure, and oxygen concentration [10,41]. Among several kinds of intermediates discussed in the literature, dioxyranyl intermediates and semiquinone intermediates are considered reactive [42,43]. In contrast, epoxide intermediates are relatively stable and unable to directly desorb from basal planes [44]. They may be involved in the indirect desorption of CO_2 and are likely to reduce C–C bond which is the major energy barrier for deposition of CO and CO_2. During the formation of surface intermediates, the adsorption of oxygen and its surface diffusion play important roles [45,46]. The focus of this discussion is the role of introduced Pd and Ag in the graphite oxidation.

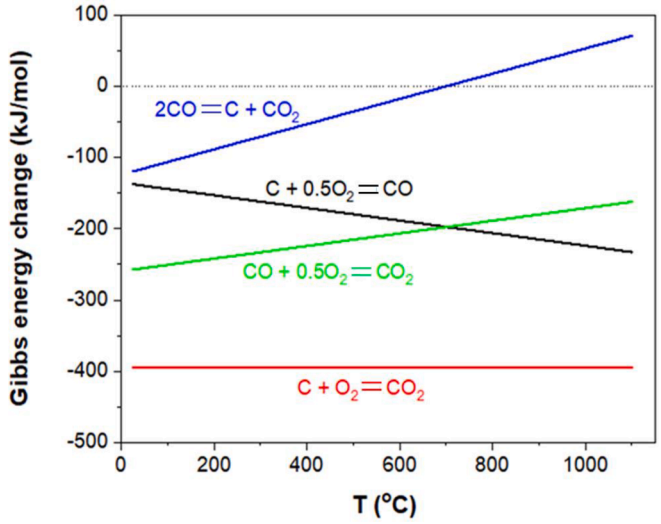

Fig. 10. Temperature dependence of Gibbs energy for major reactions involved in graphite oxidation.

The interaction of oxygen with silver surface at high temperatures and the nature of oxygen species adsorbed on Ag surfaces have been discussed in the literature [47,48]. Four types of oxygen species which were distinguished include: molecular, atomic ionic species, covalent quasi-molecular species, and Ag_2O on the surface, depending on temperatures and oxygen pressures. These oxygen species on Ag surface and subsurface were considered to exhibit different activities toward different reactions such as ethylene epoxidation and methanol to formaldehyde [49]. However, their nature is still under debate.

The reactions of metallic Ag and molecular O_2 can be written as follows:

$2Ag + 0.5O_2 = Ag_2O$(VI).

$Ag + 0.5O_2 = AgO$(VII).

Thermodynamic calculations of Gibbs energy suggest that Reaction VII is less likely in the whole temperature range, as shown in Fig. 11. The changes of Gibbs energy for Reaction VI with temperature show a dependence different than Reaction VII. At temperatures lower than approximately 630 °C, negative values are seen. At higher temperatures, the values turn positive and increase with increasing temperature. This temperature behavior suggests that the dissociative adsorption of molecular O_2 on Ag is likely, leading to the formation of Ag_2O. Compared to Reaction VI, the Gibbs energy values of Reaction VII are positive over the whole temperature range of 20 to 1000 °C, suggesting that the formation of AgO is less likely. Therefore, the surface of Ag could be free of stable oxides at temperatures considerably higher than 630 °C.

Ag_2O is likely to react with CO and C to generate CO and CO_2 via the following Reactions VIII to X since they are thermodynamically favored (shown in Fig. 11).

$Ag_2O + C = 2Ag + CO$(VIII).

$Ag_2O + 0.5C = 2Ag + 0.5CO_2$(IX).

$Ag_2O + CO = 2Ag + CO_2$(X).

Therefore, Reactions VII to X indicate that Ag is likely to be an effective catalyst towards the oxidation of graphite to CO_2 through the formation of active Ag_2O intermediate at temperatures lower than 630 °C. This is consistent with the results shown in Fig. 6(C) and Fig. 8 (A) and (B), clearly demonstrating that CO_2 is the dominant product. The catalytic oxidation of CO and carbon nanotube by Ag was recently examined [50,51]. For the CO oxidation reaction, the activity of Ag nanoparticles was correlated to the Ag-O interaction strength and Ag surface area [50]. During the oxidation of carbon nanotube, both theoretical and experimental studies suggest that the molecular O_2 dissociate on the surface of Ag nanoparticles and diffuse through the nanoparticles to reach the Ag-C interfaces and subsequently the carbon [51]. Once the C atoms on the carbon nanotube were oxidized, an oxygen concentration gradient is likely to develop inside the nanoparticles to establish a dynamic equilibrium. The oxygen species far from the Ag-C interface will supply this consumption by transiting oxygen species to the interface, driven by the oxygen concentration gradient within the nanoparticles. Because graphite and carbon nanotube are carbon materials, it is reasonably postulated that Ag nanoparticles on graphite could similarly promote the dissociation of molecular O_2 and the diffusion of dissociated oxygen species, although the nature of very active oxygen species is still unclear. According to the temperature dependence of the CO_2 fraction shown in Fig. 8(A), the dominant oxidation of IG-110 to CO_2 at temperatures lower than approximately 630 °C is likely to be promoted by the generation and diffusion of very active oxygen species on Ag. At higher temperatures, the formation of Ag_2O becomes thermodynamically formidable, leading to a decrease in the amount of active oxygen species. It is expected that the role of Ag will gradually change from an efficient catalyst to a standby observer since no oxides will be present on the Ag surface at temperatures higher than approximately 630 °C. In this case, the oxidation behavior of Ag-IG110 becomes similar to that of IG-110. This postulation is supported by the experimental results: the temperature dependence of the molar content of CO_2 at temperatures higher than 775 °C shown in Fig. 8(A) and similar linear relations for IG-110 and Ag-IG110 in Fig. 9.

Analogous to the roles of Ag in the oxidation of graphite, Pd is likely to interact with O_2, C, and CO through Reactions XI to XIV as follows:

$Pd + 0.5O_2 = PdO$(XI).

$PdO + 0.5C = Pd + 0.5CO_2$(XII).

$PdO + C = Pd + CO$(XIII).

$PdO + CO = Pd + CO_2$(XIV).

The variations of Gibbs energy for these reactions as a function of temperature are shown in Fig. 12. The values for Reaction XI remain negative until the temperature is increased to approximately 880 °C. Based on the values for Reactions XII to XIV, PdO can be reduced spontaneously to Pd by C and CO, leading to the formation of CO and CO_2. Therefore, Pd is likely to effectively catalyze the oxidation of graphite to CO_2 through the formation of PdO intermediate as the temperatures are lower than 880 °C. The catalytic oxidation of CO by Pd has been extensively studied at ambient pressure. The most active catalysts—based on highly dispersed Pd nanoparticles with optimized sizes and shapes on appropriate support—enable the oxidation of CO at low temperatures down to even room temperature [31]. In contrast, the catalytic oxidation of graphite has seen limited investigation [31,52]. Although Pd is likely to enable the dissociation of molecular O_2 through

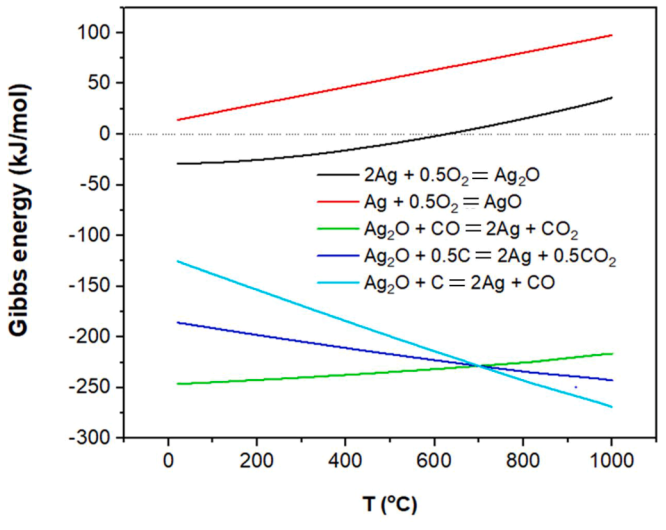

Fig. 11. Changes of Gibbs energy for reactions involving Ag in graphite oxidation as a function of temperature.

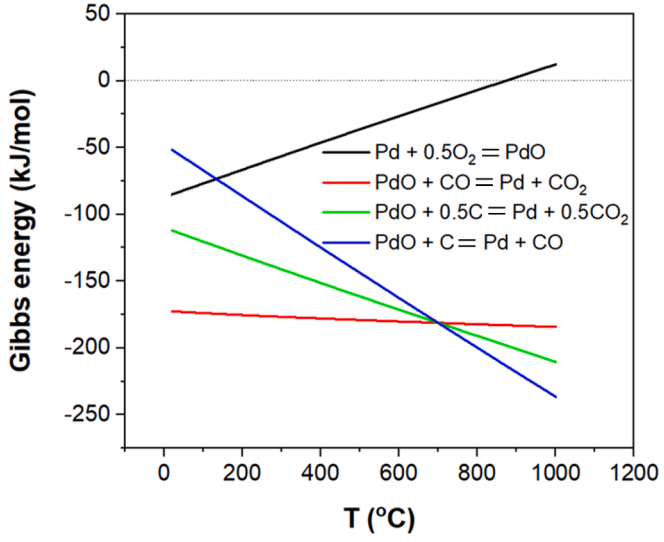

Fig. 12. Temperature dependence of Gibbs energy for reactions involving Pd in graphite oxidation.

the formation of PdO (Reaction XI), the activity of the bonded oxygen may be not sufficiently high to oxidize C through Reactions XII and XIII. Several groups observed the existence of oxygen species bound more strongly than the usual chemisorbed oxygen on Pd [53,54], which were assigned to surface oxides or dissolved oxygen in Pd. It is expected that increasing temperatures increases the activity of Pd. CO can also be catalytically oxidized to CO_2 by Pd, accompanied by the direct oxidation of graphite to CO_2. Molecular beam studies with a CO + O_2 mixture suggests that a partially oxidized Pd surface might be the reason for its oxidation capacity at high temperatures [55,56]. This could be correlated to the considerable drop of CO concentration shown in Fig. 6(B), compared to the change of CO concentration on IG-110 shown in Fig. 6 (A). With further increasing temperature, the reactivity of the bonded oxygen is likely to gradually increase until it can rapidly react with C. In this case, the role of Pd in the temperature of approximately 800 to 900 °C becomes similar to that of Ag over 400 to 500 °C. In addition, catalytic effects of Pd toward the gasification of C in CO_2 (Reaction II) over 700 to 1000 °C was also reported [57]. Therefore, the complicated temperature dependence of molar ratio of CO_2 to CO for Pd-IG110 shown in Fig. 9 may be related to multifunctional catalytic effects of Pd to several different reactions in this temperature range.

4. Conclusions

Two simulated metallic fission products known to transport - to a limited extent - through intact TRISO particles at temperatures higher than 1100 °C, Ag and Pd, exhibit pronounced catalytic effects towards the oxidation of nuclear graphite IG-110. The introduction of Ag nanoparticles to IG-110 decreases the onset temperature of the oxidation reaction from approximately 650 to 400 °C. In the temperature range of 400 to 650 °C, Ag can effectively catalyze the oxidation of IG-110 to CO_2. It is suggested that Ag is likely to promote the formation of very active oxygen species that can oxidize C to CO_2 through the dissociative absorption of molecular O_2. At temperatures beyond this range, the role of Ag gradually changes from an efficient catalyst to a standby observer because the dissociative absorption of molecular O_2 by Ag becomes thermodynamically forbidden. In contrast to Ag, Pd may play multifunctional roles in the oxidation of graphite. Pd is likely to promote the dissociative absorption of molecular O_2, leading to the formation of very reactive oxygen which oxidizes C to CO_2. But this occurs at temperatures higher than approximately 830 °C. At lower temperatures, Pd could effectively catalyze the oxidation of the intermediate or product CO to CO_2. But the graphite oxidation is limited by the reactivity of dissociated oxygen through the formation of PdO. In addition, Pd is also likely to catalyze the reaction of CO_2 and C at temperatures higher than around 700 °C. These results will be useful to assess the consequences of air ingress during the operation of HTGRs.

Simultaneous measurements of CO_2 and CO concentrations by mass spectroscopy and CO analyzer enable the separate calculations of activation energy for the formation of CO and CO_2, and the analysis of their molar ratio in the product as a function of reaction temperature. This information is also useful for the analysis of the graphite oxidation under air ingress, as well as the elucidation of the mechanism of oxidation reactions which may be involved.

The results presented are useful for assessing air ingress scenarios for an HTGR. The developed measurement provides insight into how this can alter the atmosphere in the reactor core by changing it from air to various volatile products. Future work will employ this method to quantify the influence of ingress air and moisture on graphite oxidation at higher temperatures including neutron-irradiated graphite, and further investigate catalytic effects of graphite and other TRISO materials by fission products.

CRediT authorship contribution statement

Junhua Jiang: Conceptualization, Investigation, Formal analysis, Writing – review & editing. **John Stempien:** Conceptualization, Formal analysis, Writing – review & editing. **Yaqiao Wu:** Investigation, Formal analysis.

Declaration of Competing Interest

The authors declare that they have no known competing financial interests or personal relationships that could have appeared to influence the work reported in this paper.

Data availability

Data will be made available on request.

Acknowledgement

This work is financially supported by Advanced Gas Reactor (AGR) program of the US Department of Energy, Office of Nuclear Energy under Idaho Operations Office (DE-AC07-05ID14517). The authors thank Eric Larson and Nick Smith for their technical support for developing the integrated furnace-mass spectroscopy system, and Zachary Thompson for providing ball-milled IG-110 samples.

References

[1] J. Lee, T. Ghosh, S. Loyalka, Oxidation rate of graphitic matrix material in the kinetic regime for VHTR air ingress accident scenarios, J. Nucl. Mater. 451 (2014) 48–54.
[2] K. Minato, T. Ogawa, S. Kashimura, K. Fukuda, I. Takahashi, M. Shimizu, Y. Tayama, Carbon monoxide-silicon carbide interaction in HTGR fuel particles, J. Mater. Sci. 26 (1991) 2379–2388.
[3] R. Yan, Y. Dong, Y. Zhou, X. Sun, Z. Li, Investigation of oxidation behaviors of nuclear graphite being developed and IG-110 based on gas analysis, J. Nucl. Sci. Technol. 54 (2017) 1168–1177.
[4] X. Yan, T. Takeda, T. Nishihara, K. Ohashi, K. Kunitomi, N. Tsuji, A study of air ingress and its prevention in HTGR, Nucl. Technol. 163 (2008) 401–415.
[5] R. Smith, J. Kane, W. Windes, Determining the acute oxidation behavior of several nuclear graphite grades, J. Nucl. Mater. 545 (2021), 152648.
[6] E. Kim, H. No, Experimental study on the oxidation of nuclear graphite and development of an oxidation model, J. Nucl. Mater. 349 (2006) 182–194.
[7] W. Huang, S. Tsai, I. Chiu, C. Chen, J. Kai, The oxidation effects of nuclear graphite during air-ingress accidents in HTGR, Nucl. Eng. Des. 271 (2014) 270–274.
[8] C. Contescu, S. Azad, D. Miller, M. Lance, F. Baker, T. Burchell, Practical aspects for characterizing air oxidation of graphite, J. Nucl. Mater. 381 (2008) 15–24.
[9] Y. Zhou, Y. Dong, H. Yin, Z. Li, R. Yan, D. Li, Z. Gu, X. Sun, L. Shi, Z. Zhang, characterizing thermal-oxidation behaviors of nuclear graphite by combining O_2 supply and micro surface area of graphite, Sci. Rep. 8 (2018) 13400.
[10] J. Kane, C. Contescu, R. Smith, G. Strydom, W. Windes, Understanding the reaction of nuclear graphite with molecular oxygen: Kinetics, transport, and structural evolution, J. Nucl. Mater. 493 (2017) 343–367.
[11] I. Lo, A. Tzelepi, E. Patterson, T. Yeh, A study of the relationship between microstructure and oxidation effects in nuclear graphite at very high temperatures, J. Nucl. Mater. 501 (2018) 361–370.
[12] J. Kane, C. Karthik, R. Ubic, W. Windes, D. Butt, An oxygen transfer model for high purity graphite oxidation, Carbon 59 (2013) 49–64.
[13] J. Gao, W. Yao, Y. Ma, Analytical and numerical study of graphite IG-110 parts in advanced reactor under high temperature and irradiation, Nucl. Eng. Des. 305 (2016) 421–432.
[14] R. Paul, J. Arregui-Mena, C. Contescu, N. Gallego, Effect of microstructure and temperature on nuclear graphite oxidation using the 3D random pore model, Carbon 191 (2022) 132–145.
[15] R. Morris, C. Baldwin, P. Demkowicz, J. Hunn, E. Reber, Performance of AGR-1 high-performance reactor fuel during post-irradiation heating tests, Nucl. Eng. Des. 306 (2016) 24–35.
[16] M. Barrachin, R. Dubourg, M. Kissane, V. Ozrin, Progress in understanding fission-product behavior in coated uranium-dioxide fuel particles, J. Nucl. Mater. 385 (2009) 372–386.
[17] B. Collin, D. Petti, P. Demkowicz, J. Maki, Comparison of silver, cesium, and strontium release predictions using PARFUME with results from the AGR-1 irradiation experiment, J. Nucl. Mater. 466 (2015) 426–442.
[18] S. Dwaraknath, G. Was, Development of a multi-layer diffusion couple to study fission product transport in β-SiC, J. Nucl. Mater. 444 (2014) 170–174.
[19] M. Simones, M. Reinig Jr., S. Loyalka, A mathematical model for the release of noble gas and Cs from porous nuclear fuel based on VEGA 1&2 experiments, J. Nucl. Mater. 448 (2014) 217–229.
[20] T. Weilert, K. Walton, S. Loyalka, J. Brockman, Measurements of effective Sr diffusion coefficients in IG-110 graphite, J. Nucl. Mater. 555 (2021), 153102.

[21] R. Moormann, Fission product transport and source terms in HTRs: Experience from AVR pebble bed reactor, Sci. Technol. Nucl. Install. 597491 (2008).
[22] T. Gerczak, B. Leng, K. Sridharan, J. Hunter Jr., A. Giordani, T. Allen, Observations of Ag diffusion in ion implanted SiC, J. Nucl. Mater. 461 (2015) 314–324.
[23] W. Zhang, Z. Jiao, C. Zhang, L. He, G. Xu, X. Chen, B. Liu, Diffusion of fission products in nuclear graphite: A review, Nucl. Mater. Energy 29 (2021), 101100.
[24] T. Lilloa, I. van Rooyen, Associations of Pd, U and Ag in the SiC layer of neutron irradiated TRISO fuel, J. Nucl. Mater. 460 (2015) 97–106.
[25] E. Olivier, J. Neethling, The role of Pd in the transport of Ag in SiC, J. Nucl. Mater. 432 (2013) 252–260.
[26] T. Weilert, K. Walton, S. Loyalka, J. Brockman, Effective diffusivity of Ag and migration of Pd in IG-110 graphite, J. Nucl. Mater. 559 (2022), 153427.
[27] A. Londono-Hurtado, I. Szlufarska, R. Bratton, D. Morgan, A review of fission product sorption in carbon structures, J. Nucl. Mater. 425 (2012) 254–267.
[28] K. Walton, N. Jacobson, B. Kowalski, J. Brockman, S. Loyalka, Sorption isosteres and isotherms of silver on NBG-17 graphite, J. Nucl. Mater. 557 (2021), 153264.
[29] D. McKee, Metal oxides as catalysts for the oxidation of graphite, Carbon 8 (1970) 623–635.
[30] E. Turkdogan, J. Vinters, Catalytic oxidation of carbon, Carbon 10 (1972) 97–111.
[31] B. Baker, J. France, L. Rouse, R. Waite, Catalytic oxidation of graphite by platinum and palladium, J. Catal. 41 (1976) 22–29.
[32] S. Dey, G. Dhal, Applications of silver nanocatalysts for low-temperature oxidation of carbon monoxide, Inorg. Chem. Commun. 110 (2019), 107614.
[33] A. Roine, HSC Chemistry® [Software], Pori Software, 2018.
[34] H. Wu, R. Gakhar, A. Chen, S. Lam, C. Marshall, R. Scarlat, Comparative analysis of microstructure and reactive sites for nuclear graphite IG-110 and graphite matrix A3, J. Nucl. Mater. 528 (2020), 151802.
[35] S. Navaladian, B. Viswanathan, T. Varadarajan, R. Viswanath, A rapid synthesis of oriented palladium nanoparticles by UV irradiation, Nanoscale Res. Lett. 4 (2009) 181–186.
[36] M. Khan, S. Kumar, M. Ahamed, S. Alrokayan, M. AlSalhi, Structural and thermal studies of silver nanoparticles and electrical transport study of their thin films, Nanoscale Res. Lett. 6 (2011) 434.
[37] A. Monshi, M. Foroughi, M. Monshi, Modified Scherrer equation to estimate more accurately nano-crystallite size using XRD, World J. Nano Sci. Eng. 2 (2012) 154–160.
[38] J. Lee, T. Ghosh, S. Loyalka, Comparison of NBG-18, NBG-17, IG-110 and IG-11 oxidation kinetics in air, J. Nucl. Mater. 500 (2018) 64–71.
[39] J. Arthur, Reactions between carbon and oxygen, Trans. Faraday Soc. 47 (1951) 164–178.
[40] M. Takahashi, M. Kotaka, H. Sekimoto, Burn-off and production of CO and CO_2 in the oxidation of nuclear reactor-grade graphites in a flow system, J. Nucl. Sci. Technol. 31 (1994) 1275–1286.
[41] A. Theodosiou, A. Jones, B. Marsden, Thermal oxidation of nuclear graphite: A large scale waste treatment option, PLoS One 12 (2017) e0182860.
[42] C. Li, X. Chen, L. Shen, N. Bao, Revisiting the oxidation of graphite: Reaction mechanism, chemical stability, and structure self-regulation, ACS Omega 5 (2020) 3397–3404.
[43] A. Sánchez, F. Mondragón, Role of the epoxy group in the heterogeneous CO_2 evolution in carbon oxidation reactions, J. Phys. Chem. C 111 (2007) 612–617.
[44] N. Laine, F. Vastola, P. Walker, The importance of active surface area in the carbon-oxygen reaction, J. Phys. Chem. 67 (1963) 2030–2034.
[45] R. Batchu, Z. Thompson, Z. Fang, W. Windes, E. Dufek, R. Fushimi, Role of surface diffusion in formation of unique reactivity for graphite oxidation: Time-resolved measurements in a pulsed diffusion reactor, Carbon 182 (2021) 781–790.
[46] J. Hahn, H. Kang, S. Lee, Y. Lee, Mechanistic study of defect-induced oxidation of graphite, J. Phys. Chem. B 103 (1999) 9944–9951.
[47] E. Ivanov, A. Boronin, S. Koscheeve, G. Zhidomirov, Modeling of oxygen adsorption on silver, React. Kinet. Catal. Lett. 66 (1999) 265–272.
[48] J. Wang, W. Dai, J. Deng, X. Wei, Y. Cao, R. Zhai, Interaction of oxygen with silver surface at high temperature, Appl. Surf. Sci. 126 (1998) 148–152.
[49] G. Millar, J. Metson, G. Bowmaker, R. Cooney, In situ Raman studies of the selective oxidation of methanol to formaldehyde and ethene to ethylene oxide on a polycrystalline silver catalyst, J. Chem. Soc., Faraday Trans 91 (1995) 4149–4159.
[50] M. Lamoth, M. Plodinec, L. Scharfenberg, S. Wrabetz, F. Girgsdies, T. Jones, F. Rosowski, R. Horn, R. Schlögl, E. Frei, Supported Ag nanoparticles and clusters for CO oxidation: size effects and influence of the silver–oxygen interactions, ACS Appl. Nano Mater. 2 (2019) 2909–2920.
[51] Y. Yue, D. Yuchi, P. Guan, J. Xu, L. Guo, J. Liu, Atomic scale observation of oxygen delivery during silver-oxygen nanoparticles catalyzed oxidation of carbon nanotubes, Nat. Commun. 7 (2016) 12251.
[52] J. Fryer, Oxidation of graphite catalyzed by palladium, Nature 220 (1968) 1121–1122.
[53] M. Milun, P. Pervan, K. Wandelt, Interaction of oxygen with a polycrystalline palladium surface over a wide temperature range, Surf. Sci. 218 (1989) 363–388.
[54] J. Gegner, G. Hörz, R. Kirchheim, Diffusivity and solubility of oxygen in solid palladium, J. Mater. Sci. 44 (2009) 2198–2205.
[55] S. Shaikhutdinov, M. Heemeier, J. Hoffmann, I. Meusel, B. Richter, M. Bäumer, H. Kuhlenbeck, J. Libuda, H. Freund, R. Oldman, S. Jackson, C. Konvicka, M. Schmid, P. Varga, Interaction of oxygen with palladium deposited on a thin alumina film, Surf. Sci. 501 (2002) 270–281.
[56] C. Gopinath, K. Thirunavukkarasu, S. Nagarajan, Kinetic evidence for the influence of subsurface oxygen on palladium surfaces towards CO oxidation at high temperatures, Asian J. Chem. 4 (2009) 74–80.
[57] Y. Tamai, H. Watanabe, A. Tomita, Catalytic gasification of carbon with steam, carbon dioxide and hydrogen, Carbon 15 (1977) 103–106.